Electronic Supplementary Information

Elucidating mechanochemical reactivity of a ternary halogen-bonded cocrystal system explained by computational studies and calorimetry

Lavanya Kumar,[a]† Sibananda G. Dash,[a]† Katarina Leko,[b] Damian Trzybiński, [c] Nikola Bregović,[b*] Dominik Cinčić,[b*] M. Arhangelskis[a*]

[a] Faculty of Chemistry, University of Warsaw, 1 Pasteura Street, Warsaw 02-093, Poland.

[b] Faculty of Science, Department of Chemistry, University of Zagreb, Horvatovac

102a, HR-10000 Zagreb, Croatia.

[c] Biological and Chemical Research Centre, University of Warsaw, Żwirki i Wigury

101, 02-089 Warsaw, Poland.

Corresponding authors: nbregovic@chem.pmf.hr; dominik@chem.pmf.hr; m.arhangelskis@uw.edu.pl.

Table of Contents

S1 Materials and Methods

S1.1 Materials

The **tftib** was purchased from **Alfa Aesar,** whereas **tpss** and **pyr** were procured from **Sigma Aldrich**. The solvents used in the crystallisation were of HPLC grade and purchased from **POCH**. All the chemicals were used without further purification.

S1.2 Mechanochemical ball-milling experiments

Milling reactions were performed using Retsch MM400 shaker mill equipped with 10 ml stainless steel-jar with two 7 mm steel balls at 30 Hz frequency for 30 minutes. The reactants were mixed in a stoichiometric ratio and scaled to the total mass of 200 mg. 10 μl of ethanol liquid was added to the reaction mixture, which was then milled for 30 minutes. Milled products were dried in open air and characterised by PXRD.

S1.3 Powder X-ray diffraction (PXRD) measurements

The structures of the materials obtained from the mechanochemical grinding were confirmed using powder X-ray diffraction (PXRD) measurements. The measurements were performed on a Bruker D8 Advance diffractometer equipped with a *Lynxeye* detector and Cu*K*α (λ= 1.54184 Å) source operating at 40 kV and 40 mA by scanning over a 2θ range of 3 – 40 degrees with a step size of 0.04°.

S1.4 Single-crystal X-ray diffraction (SCXRD) measurements

The crystals of (**tftib**)(**pyr**)½(**tpss**)½ (**3-comp**) suitable for crystallographic analysis were grown by slow evaporation from acetonitrile solution. Good quality single-crystal was selected for the X-ray diffraction measurement at T = 100(2) K. The crystal was mounted with paratone-N oil on a MiTeGen micromount. Diffraction data were collected on the Agilent Technologies Super Nova Single Source diffractometer with Mo*K*α radiation (λ = 0.71073 Å) using CrysAlis Pro software.[1] The analytical numeric absorption correction using a multifaceted crystal model based on expressions derived by R.C. Clark & J.S. Reid was applied.[2] The structure determination procedure was carried out using the SHELX package.[3] The structure was solved with direct methods and then successive least-square refinement was carried out based on the full-matrix least-squares method on F^2 in SHELXL.[3] The H-atoms were positioned geometrically, with C–H bond length equal to 0.93 Å, and constrained to ride

on their parent atoms with $U_{iso}(H) = 1.2U_{iso}(C)$. The figures for this publication were prepared using Mercury[4] software.

S1.5 Thermogravimetric analysis (TGA) and differential scanning calorimetry (DSC) measurements

Between 2-10 mg of each sample (exact mass) were weighed using Mettler-Toledo XS105 Dual Range balance and placed into a standard 70 µl alumina crucible. The TGA/DSC analysis was performed using the Mettler-Toledo TGA/DSC STAR^e system under a constant flow of dry N_2 (60 ml/min), with a heating rate of 10ºC/min over a temperature range of 30 to 300 °C.

S1.6 Dissolution calorimetry measurements

The dissolution enthalpies of **tpss**, **(tftib)(tpss)** and **3-comp** were determined calorimetrically in acetonitrile at 25°C using TAM IV calorimeter (TA Instruments). The solid sample (m = 2.5 –3.5 mg) and 15 ml acetonitrile solvent (HPLC grade, Fischer Chemicals) were placed in the sample cartridge and calorimeter cell, respectively. Then the cell was mounted inside the calorimeter and allowed to reach thermal equilibrium overnight, while stirring at 60 rpm. The equilibration criteria were set as follows: heat flow (baseline slope within 30 min) < 500 nW/h, heat flow standard deviation < 100 nW. The sample was exposed to the solvent by releasing the sample cartridge into the calorimeter cell after the baseline equilibration period. Integration of the heat flow was used to obtain the total heat associated with the dissolution process. Finally, the enthalpy of dissolution was measured by subtracting the heat signal for blank samples. The experiments were performed in triplicate. (see Table S8-S9 and Fig. S9-S11). The dissolution enthalpies for **pyr**, **tftib** and **(tftib)(pyr)$_{1/2}$** were taken from our previous work.[5]

S2 Cambridge Structural Database (CSD) search

A survey of Cambridge Structural Database (version: 2022.3.0)[6] was performed for the potential sulfur containing coformers for **tftib**. The CSD search for the reported binary cocrystals of substituted iodobenzenes was analysed and the coformers that form I···S interactions were considered only. The following conditions were used during the CSD search: *only organic*, *only single crystal structures*. The results of the database analysis are given in **Table S1**.

Table S1. CSD search for the sulfur containing cocrystals of halobenzenes.

Halogen Bond Donor	Hits (cocrystals)	No. of S-containing coformers	Coformers
Iodobenzene	102	0	-
Pentafluoro Iodobenzene	96	2	***Triphenyl phosphine sulfide***, 4H-[1,4'-bipyridine]-4-thione
1,4-diiodobenzene	32	0	-
1,4-diiodo tetrafluorobenzene	511	30	1-t-butyl-1,3-dihydro-2H-imidazole-2-thione, 1,3-dithiane, 1,4-dithiane, methyl 4-(2-chlorophenyl)-6-methyl-2-sulfanylidene-1,2,3,4-tetrahydropyrimidine-5-carboxylate, 1,3-thiazolidine-2-thione, N,N-diphenylthiourea, N,N'-dimethylthiourea, N,N,N',N'-tetramethylthiourea, 4,5-bis(methylsulfanyl)-2H-1,3-dithiole-2-thione, 5-(trifluoromethyl)pyridine-2(1H)-thione, thiomorpholine, 2-Mercapto-1-methyl-imidazole, benzenecarbothioamide, 2-methylbenzenecarbothioamide, 3-methylbenzenecarbothioamide, 4-methylbenzenecarbothioamide, 2-methoxybenzenecarbothioamide, 3-methoxybenzenecarbothioamide, 4-methoxybenzenecarbothioamide, 3-nitrobenzenecarbothioamide, 2-fluorobenzenecarbothioamide, 2-chlorobenzenecarbothioamide, 4-chlorobenzenecarbothioamide, p-tolyl sulfoxide, Carbimazole, ***Triphenyl phosphine sulfide***, thiobenzamide, N-(morpholin-4-yl)thian-4-imine, thian-4-one,

1,2-diiodo tetrafluorobenzene	103	14	1,4-dithiane, imidazolidine-2-thione, 5-(trifluoromethyl)pyridine-2(1H)-thione, 1,3-thiazolidine-2-thione, N,N'-dimethylthiourea, N,N'-diphenylthiourea, 1,3-dimethyl-2-sulfanylideneimidazolidin-4-one, 1,7,7-trimethylbicyclo[2.2.1]heptane-2-thione, 2-Mercapto-1-methyl-imidazole, N,N'-dimethylthiourea, ***Triphenyl phosphine sulfide***, 1,3-Dihydro-2H-benzimidazole-2-thione, 1,3-bis(2,4,6-trimethylphenyl)-1,3-diazepane-2-thione thiourea, 1-methylthiourea
1,3-diiodo tetrafluorobenzene	73		1,3-dithiane, 1,4-dithiane, Tetraethylammonium thiocyanate, thiourea, N,N'-dimethylthiourea, ***Triphenyl phosphine sulfide***, 1,3-bis(2,4,6-trimethylphenyl)-1,3-diazepane-2-thione
1,3,5-triiodobenzene	0	0	-
1,3,5-triiodo-2,4,6-trifluorobenzene	133	6	1,3-dithiane, 1,4-dithiane, N,N'-dimethylthiourea, ***Triphenyl phosphine sulfide***, N-[2-(morpholin-4-yl)ethyl]thian-4-imine, thian-4-one

S3 Theoretical Studies

S3.1 Periodic DFT calculations

The structure of **3-comp** obtained from single-crystal XRD experiment was used as a starting point for the periodic DFT geometry optimisation, while the structures of the other cocrystals and individual coformers were obtained from the Cambridge Structural Database (CSD).[6] The C−H bond lengths were normalised to their neutron diffraction values using Mercury,[4] after which the structures were converted into the input format of CASTEP using cif2cell utility[7] for geometry optimisation. The unit cell parameters and atomic coordinates were optimised with a constraint on crystal symmetry. The calculations were performed at 800eV plane wave basis cutoff with ultrasoft on-the-fly generated pseudopotentials, combining the PBE functional[8] with either Grimme dispersion correction (D3)[9] or many-body dispersion correction (MBD*)[10–12] using CASTEP (version 22.11)[13] code. The convergence criteria for the calculation were set as follows: energy = 2×10^{-5} eV/atom, force = 5×10^{-2} eV/Å, displacement = 10^{-3} Å, stress = 10^{-2} GPA. The energies of cocrystal formation and interconversion reactions were calculated by a similar method as adapted in our previous work.[5] The formation and interconversion energies of the cocrystals are given in Tables S3-S5.

S3.2 Molecular energy framework calculations

Interaction energy and energy framework[14] calculations were performed with *CrystalExplorer17.5*[15] software package starting from the periodic DFT optimised geometry. The calculations were performed with the B3LYP[16–18]/DGDZVP[19] method for all the molecular pairs within the sphere (20 Å) for each of the symmetry-distinct molecules in the asymmetric unit. The cylindrical tube size (scale factor) was set to 100 for all energy framework calculations.

S4 Results

S4.1 Periodic DFT calculations

Table S2. Periodic DFT calculated energy of the starting compounds.

Compound	**CSD refcode**	**Energy per primitive cell (eV)**		**Energy per formula unit (eV)**	
		D3	**MBD***	**D3**	**MBD***
tftib	UCEPEY	-21266.160	-21266.47	-5316.540	-5316.617
pyr	PYRAZI01	-2495.474	-2495.584	-1247.737	-1247.792
tpss	TPPOSS02	-28828.432	-28831.323	-3603.554	-3603.915

Table S3. Periodic DFT Calculated energy of the cocrystals.

Cocrystal	**CSD refcode**	**Energy per primitive cell (eV)**		**Energy per formula unit (eV)**		**Formation Energy (kJ/mol)**	
		D3	MBD*	D3	MBD*	D3	MBD*
(tftib)(pyr)$_{1/2}$	LICDEK	-23762.237	-23762.567	-5940.559	-5940.642	-14.53	-12.39
(tftib)(tpss)	RUWVEN	-35680.848	-35682.280	-8920.212	-8920.570	-11.38	-3.59
3-comp	This work	-30969.389	-30970.410	-7742.347	-7742.602	-15.59	-12.67

Note: All the calculations were performed using PBE method. Average energy of the **tpss** polymorphs was used in the formation energy calculation for **(tftib)(tpss)**.

Table S4. Interconversion energy (in kJ/mol) predicted by periodic DFT and dissolution calorimetry method for binary cocrystals.

Reaction equation	**Periodic DFT calculation**		**Molecular energy framework**	**Dissolution calorimetry**
(**tftib**)(**pyr**)$_{1/2}$ + **tpss** → (**tftib**)(**tpss**) + 1/2 **pyr**	PBE+MBD*	PBE+D3	13.82	8.6(7)
	8.81	3.15		

Table S5. Interconversion energies (in kJ/mol) predicted from different methods for ternary cocrystal formation.

Reaction equation	**Periodic DFT calculation**		**Molecular energy framework**	**Dissolution calorimetry**
	PBE+MBD*	PBE+D3		
(**tftib**)(**pyr**)$_{1/2}$ + 1/2 **tpss** → (**tftib**)(**pyr**)$_{½}$(**tpss**)$_{½}$	-0.28	-1.06	3.11	-5.1(7)
(**tftib**)(**tpss**)+ 1/2 **pyr** → (**tftib**)(**pyr**)$_{½}$(**tpss**)$_{½}$ + 1/2 **tpss**	-9.08	-4.21	-10.71	-13.6(5)
(**tftib**)+ 1/2 **tpss**+ 1/2 **pyr** → (**tftib**)(**pyr**)$_{½}$(**tpss**)$_{½}$	-12.67	-15.59	-15.64	-13.9(4)

Table S6. Comparison of the halogen bond lengths in the DFT-optimised and experimental cocrystal structures.

Cocrystal	**Calculated XB length / Å**		**Experimental XB length / Å**
	PBE+MBD*	**PBE+D3**	
3-comp	2.746	2.817	2.847(3)
(tftib)(pyr)$_{1/2}$	2.761	2.824	2.871(9)
(tftib)(tpss)	3.037	3.045	3.163(1)

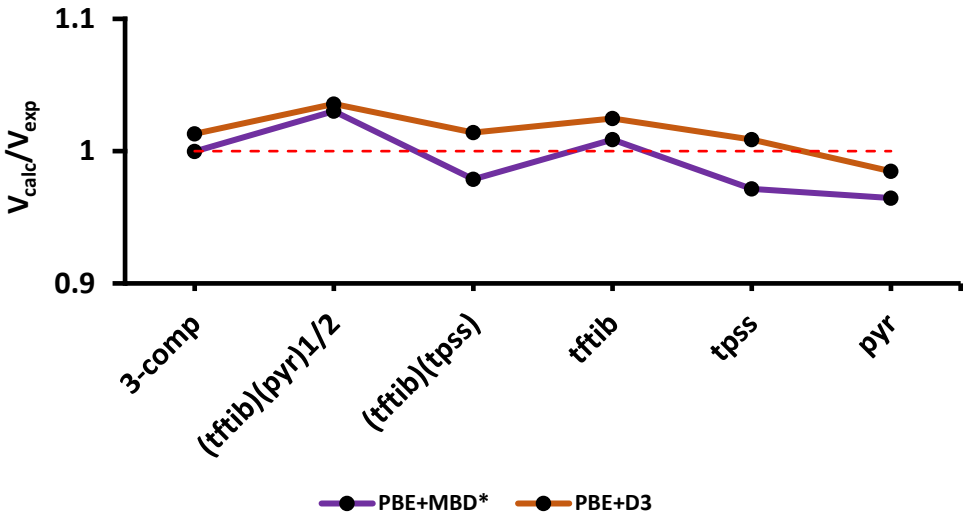

Fig. S1. Unit cell volume ratio between the DFT-optimised and experimental crystal structures of the cocrystals and starting materials. The horizontal dashed red line represents the ideal ratio of .

S4.2 Powder X-ray diffraction measurements

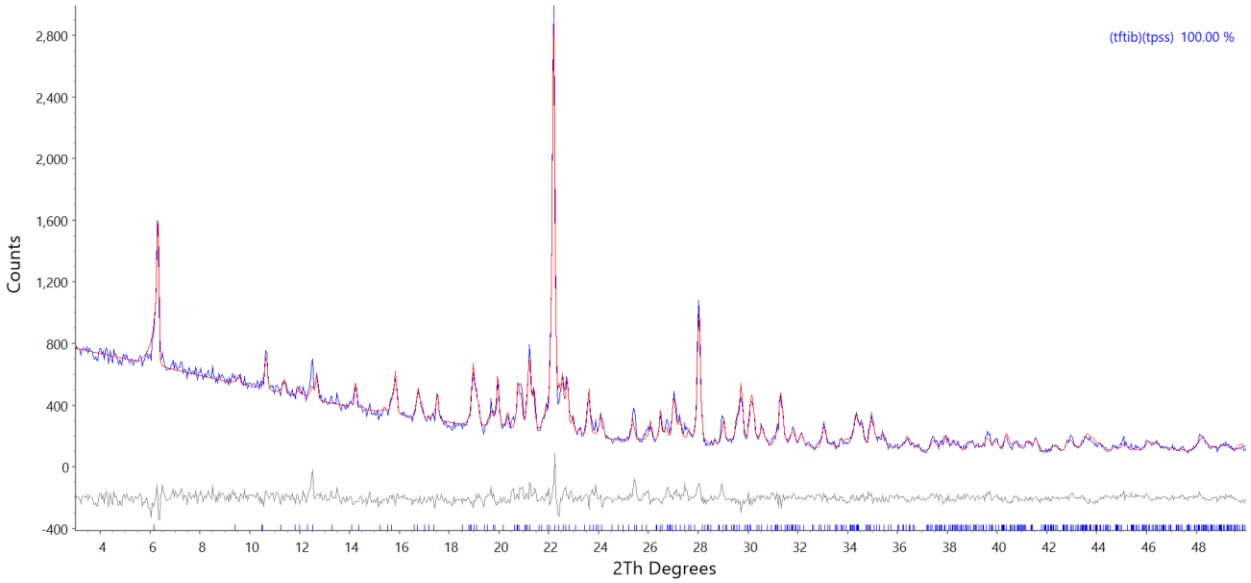

Fig. S2. Rietveld refinement of **(tftib)(tpss)** prepared for the synthesis of ternary cocrystal against the reported polymorph of **(tftib)(tpss)** cocrystal (refcode: **RUWVEN**).

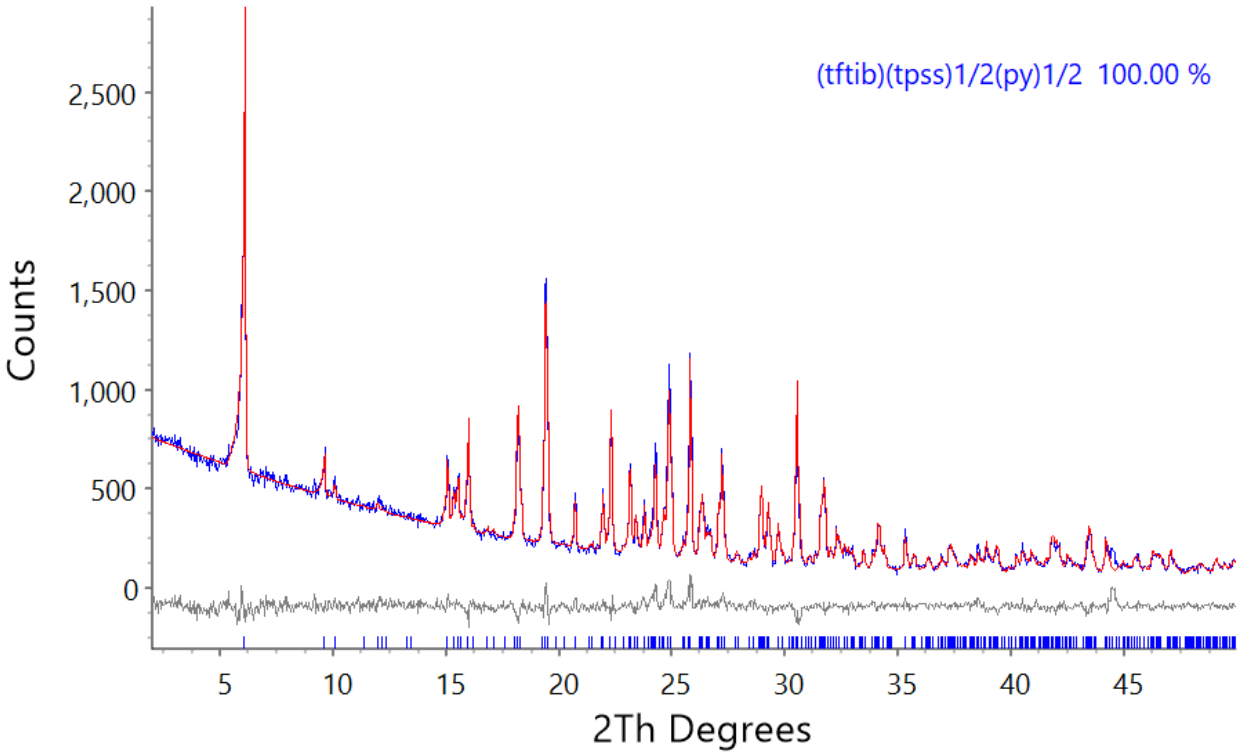

Fig. S3. Rietveld refinement of **3-comp** mechanochemically synthesised from **(tftib)(pyr)**$_{1/2}$. The experimental profile is shown in blue, calculated profile in red and their difference in the grey.

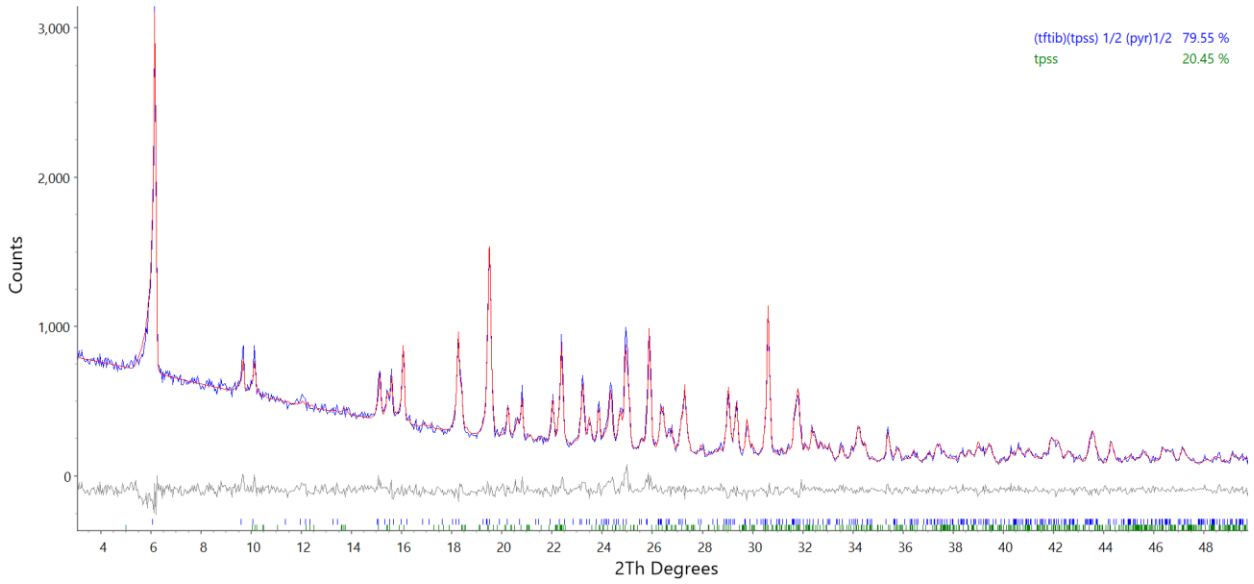

Fig. S4. Rietveld refinement of **3-comp** mechanochemically synthesised from (**tftib**)(**tpss**) in a reaction with **pyr**. The experimental profile is shown in blue, calculated profile in red and the difference in the grey.

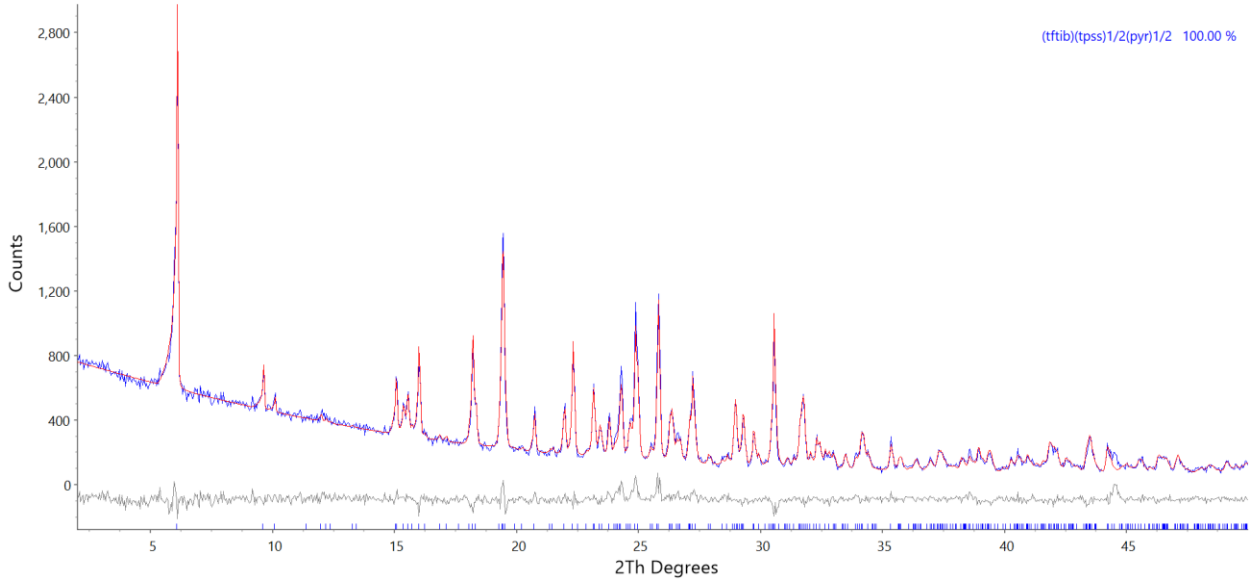

Fig. S5. Rietveld refinement of **3-comp** mechanochemically synthesised in a reaction between **tftib**, **tpss** and **pyr**. The experimental profile is shown in blue, calculated profile in red and the difference in the grey.

S4.3 Energy framework analysis

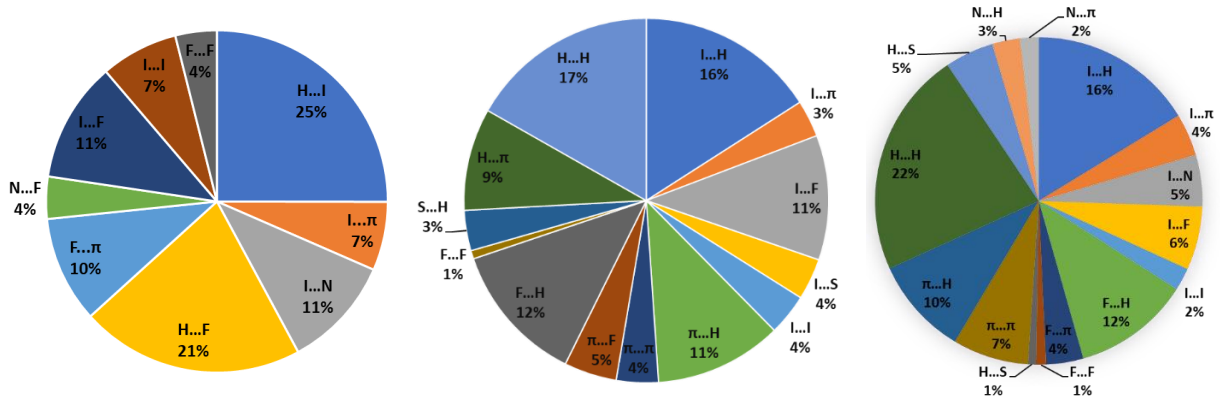

(a) **(b)** **(c)**

Fig. S6. Quantitative information of the intermolecular interactions obtained from 2D fingerprint plots present in **(a)** (**tftib**)(**pyr**)$_{1/2}$ **(b)** (**tftib**)(**tpss**) **(c) 3-comp** cocrystals.

Table S7. Total intermolecular interaction energies calculated for the molecules in the asymmetric unit of cocrystals.

(**tftib**)(**pyr**)$_{1/2}$	(**tftib**)(**tpss**)	**3-comp**
-186.7 kJ/mol	-272.8 kJ/mol	-308.4 kJ/mol

Table S8. Intermolecular interaction energies for binary and ternary cocrystals with energy cutoff -10 kJ/mol.

Crystal system	Interaction	Energy (kJ/mol)
(tftib)(pyr)$_{1/2}$	C−F···π/ C−I··· π (tftib-tftib)	-16.8 to 26.8
	C−I···N	-20.4
	C−F···π (tftib-pyr)	-16.8
(tftib)(tpss)	C−F···π/ C−I···π (tftib-tftib)	-46.5
	C−I···S (tftib-tpss)	-13.7
	C−I···π (tftib-tpss)	-33.6
3-comp	C−I···π (tftib-tpss)	-20.5
	C-H···S (pyr-tpss)	-29.6
	C−I···N (tftib-pyr)	-19.2
	C−H···π (pyr-tpss)	-19.1
	C−H···S/ π···S (tpss-tpss)	-18.6
	π···π (pyr-tpss)	-11.2
	C−H···π (tpss-tpss)	-12.7
	C−H···π (tftib-tpss)	-14.0
	C−F···π/ C−I···π (tftib-tftib)	-42.3
	C−F···π/ C−I···π (tftib-tftib)	-49.8

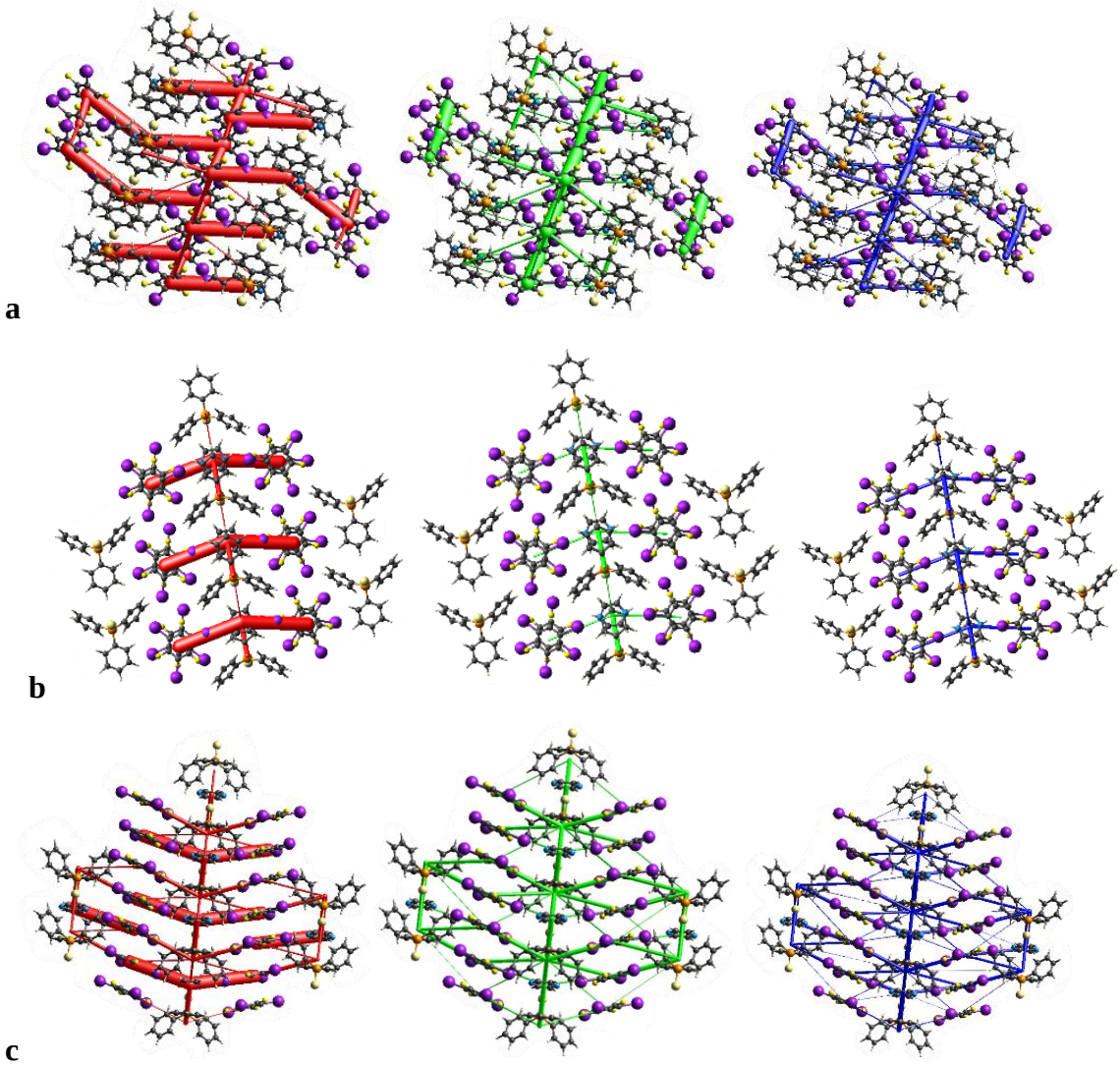

Fig. S7. Energy framework calculated for **3-comp** with respect to **(a) tftib (b) pyr (c) tpss** Electrostatic, dispersion and total energies were represented by red, green and blue colour respectively. The cylindrical radii were scaled proportional to the relative energies of the corresponding interactions. This scaling was performed using a common scale factor of 100 and a cutoff value of 3 kJ/mol.

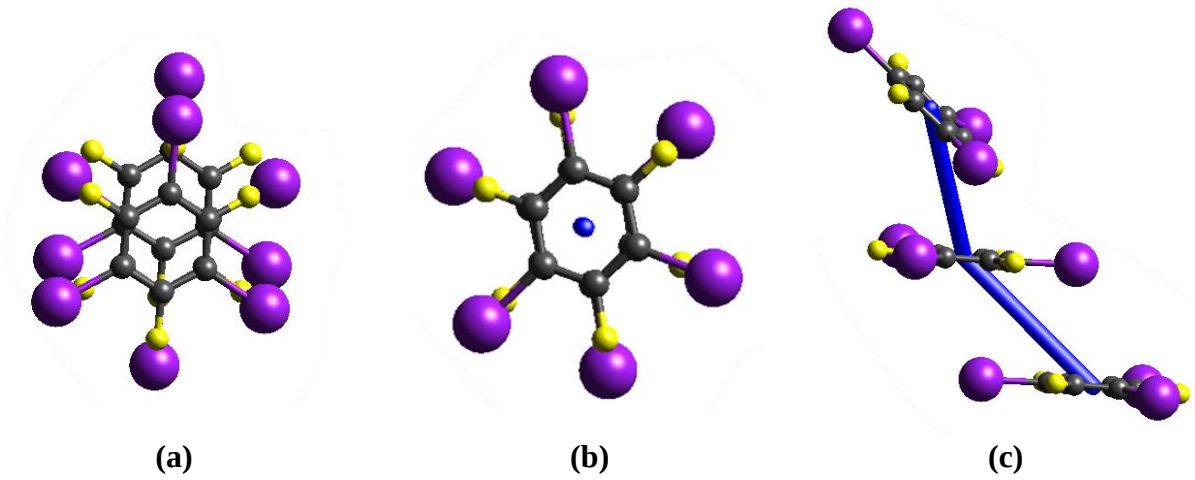

Fig. S8. Types of π-π stacking between **tftib** molecules found in the cocrystals of **(a) 3-comp**, **(b) (tftib)(tpss)**, **(c) (tftib)(pyr)**$_{1/2}$.

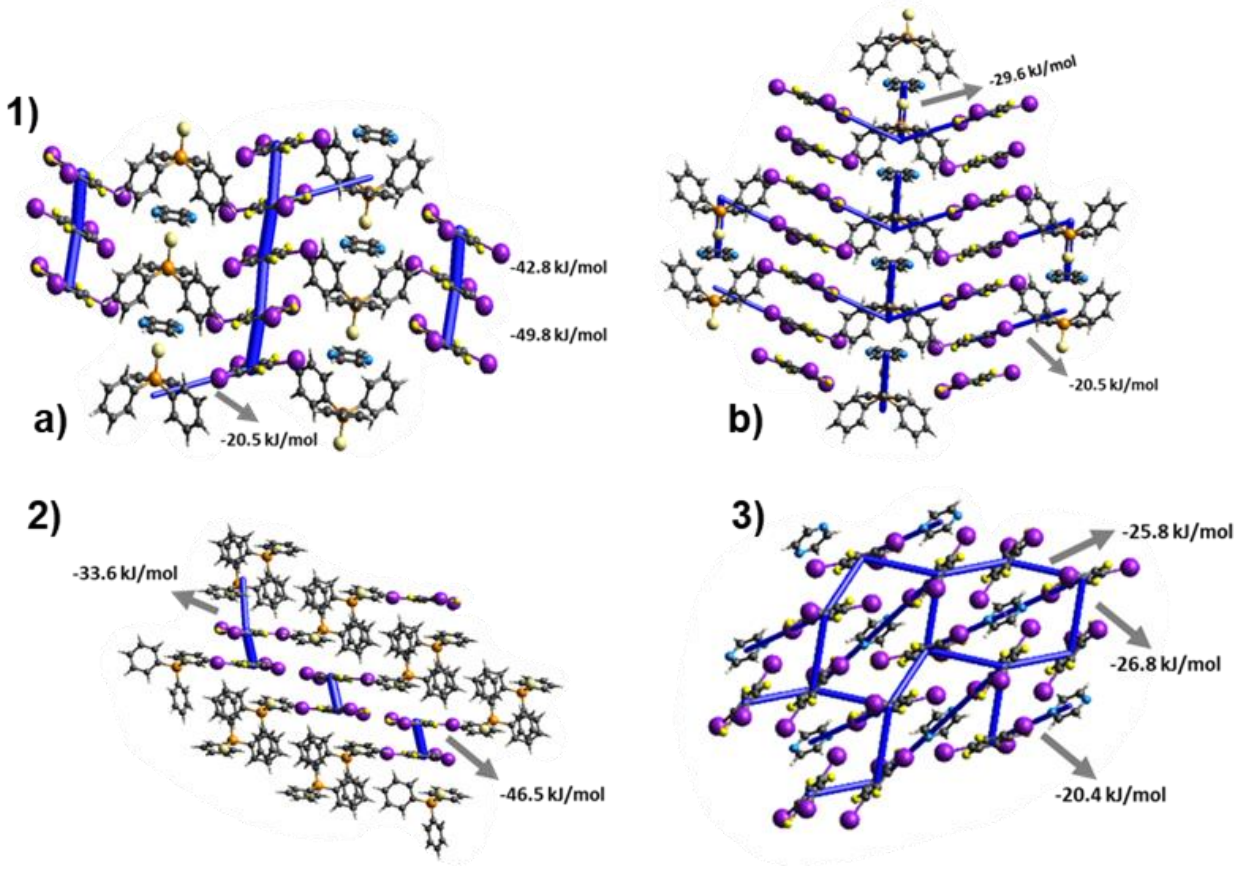

Fig. S9. Molecular energy framework **(1a)** with respect to **tftib, (1b) tpss** in **3-comp**, and for **2) (tftib)(tpss)**, **3) (tftib)(pyr)**$_{1/2}$.

S4.4 Crystallographic information

Table S9. Crystallographic data collection and structure refinement details for **3-comp**, **(tftib)(pyr)$_{1/2}$** and **(tftib)(tpss)**. The crystallographic parameters for **(tftib)(pyr)$_{1/2}$**[5] and **(tftib)(tpss)**[20] were taken from the previously reported work.

Parameters			
Cocrystal	**3-comp**	**(tftib)(pyr)$_{1/2}$**	**(tftib)(tpss)**
Molecular formula	$C_{34}H_{19}F_6I_6N_2PS$	$C_8H_2F_3I_3N$	$C_{24}H_{15}F_3I_3PS$
Formula weight	1393.94	549.81	804.09
Crystal system	Monoclinic	Monoclinic	Monoclinic
Space group	*P*21/*m*	*P*21/c	*P*21/c
Z	2	4	4
***a* (Å)**	7.2546(1)	9.1685(4)	14.2390(2)
***b* (Å)**	28.9120(4)	7.7161(3)	9.2962(2)
***c* (Å)**	9.1504(1)	16.7661(6)	18.8524(3)
***α* (°)**	90	90	90
***β* (°)**	92.873(1)	99.439(4)	98.4940(10)
***γ* (°)**	90	90	90
***V* (Å^{-3})**	1916.84(4)	1170.06(8)	2468.09(7)
ρ_{calc} (g/cm^3)	2.415	3.121	2.164
$M_{MoK\alpha}$ (mm^{-1})	5.016	8.019	3.982
***F*$_{000}$**	1280	972	1504
***T* (K)**	100(2)	100(2)	103(2)
$\theta_{min,\ max}$ (°)	2.2, 26.4	2.3, 25.1	2.2, 25.0
Total reflections	25064	13981	21528
Unique reflections	3982	2914	4337
Observed reflections (I > 2σ)	3634	2612	3589
***R*$_{int}$**	0.036	0.115	-
***R*$_1$ (*F*^{2})**	0.0207	0.0463	0.0300
w*R*$_2$ (F^2)	0.0486	0.1156	0.0468
Goodness-of-fit	1.15	1.159	1.008
$\Delta\rho_{min,\ max}$ (e Å^{-3})	-0.75, 0.75	-1.53, 1.89	-0.659,0.643
CCDC No.	2289502	2217175	1898060

S4.5 Crystal packing in binary cocrystals

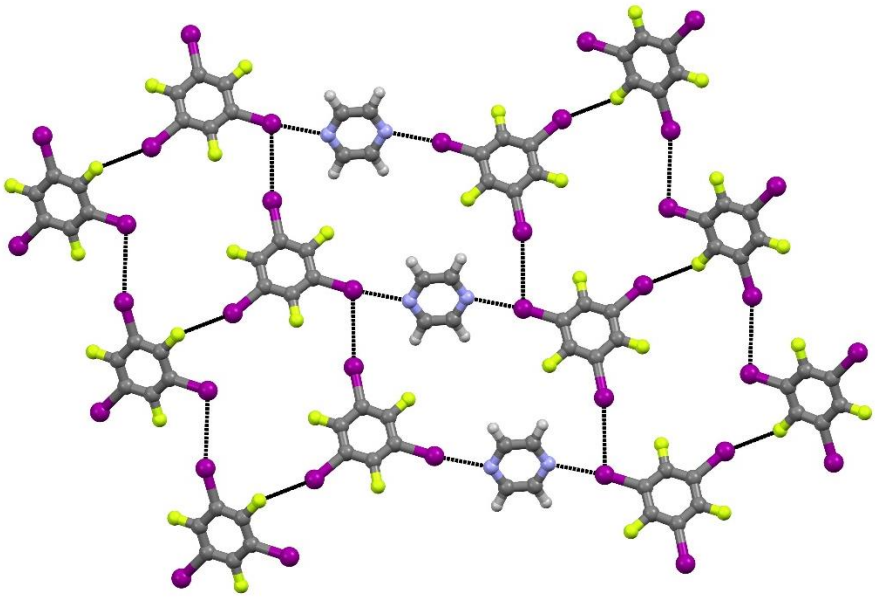

(a)

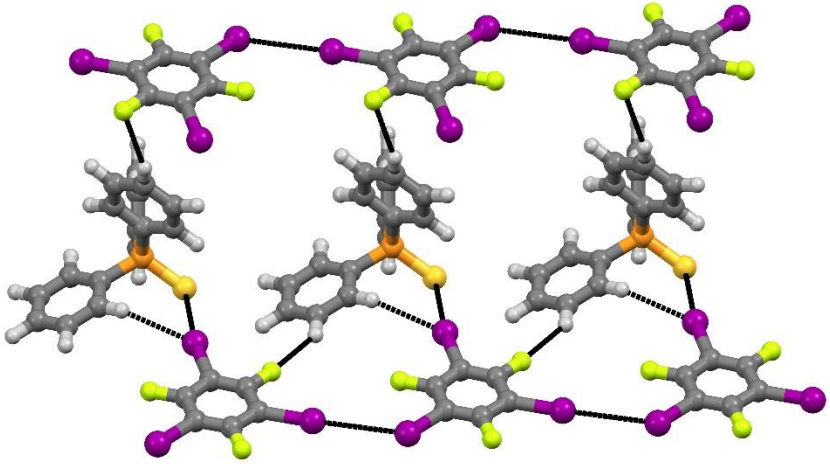

(b)

Fig. S10. Crystal packing in the **(a) (tftib)(pyr)**$_{1/2}$, and **(b) (tftib)(tpss)** cocrystals.

S4.6 Dissolution calorimetry experiments

Table S10. Dissolution enthalpies from calorimetry measurements. The measurements for 3-comp, tpss and (tftib)(tpss) were performed in this work, while dissolution enthalpies for all the other material were taken from our earlier publication.[5] Uncertainties of the last digit are given in parentheses as standard errors of the mean.

Compound	**$\Delta_s H$ / kJ mol^{-1}**	**Cocrystal Formation Enthalpy / kJ mol^{-1}**
tftib	17.4(1)	–
pyr	16.49(5)	–
tpss	29.0(2)	–
(tftib)(pyr)$_{1/2}$	34.5(5)	-8.8(5)
(tftib)(tpss)	46.6(4)	-0.2(5)
3-comp	54.0(3)	-13.9(4)

Table S11. Dissolution enthalpies of **3-comp**, **tpss and (tftib)(tpss)** in acetonitrile at 25 °C. Uncertainties of the last digit are given in parentheses as standard errors of the mean.

Material	m / mg	Q / mJ	$\Delta_s H$ / kJ mol^{-1}
3-comp	2.520	185.44	**54.0(3)**
	3.530	256.01	
	3.020	223.86	
(tpss)	7.08	697.89	**29.0(2)**
	3.03	281.69	
	6.35	607.93	
(tftib)(tpss)	2.62	138.92	**46.6(4)**
	6.12	344.91	
	4.83	268.97	

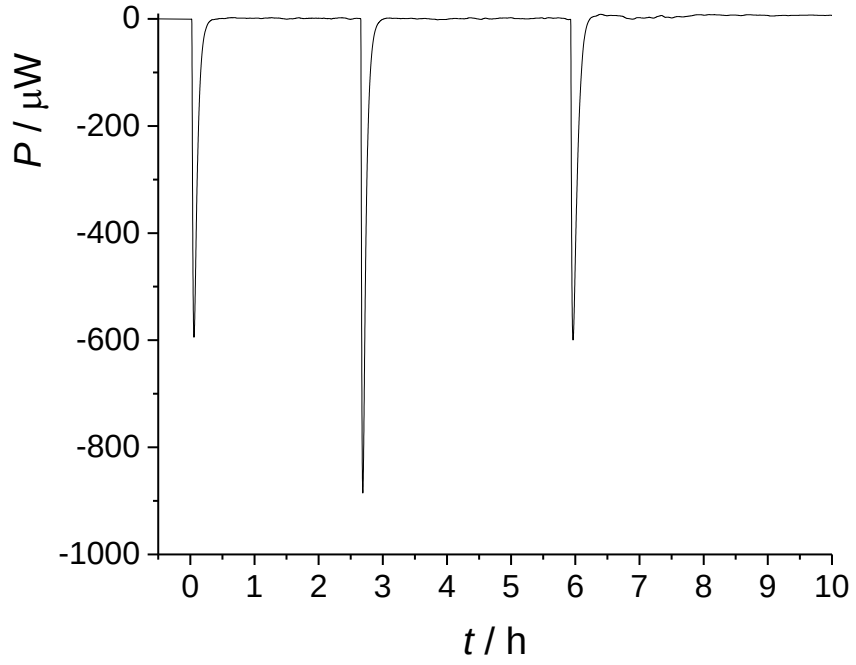

Fig. S11. Calorimetric determination of dissolution enthalpy of **(tftib)(pyr)$_{1/2}$(tpss)$_{1/2}$** (m_1=2.520 mg, m_2=3.530 mg, m_3=3.020 mg) in acetonitrile at 25°C; stirring rate = 60 rpm.

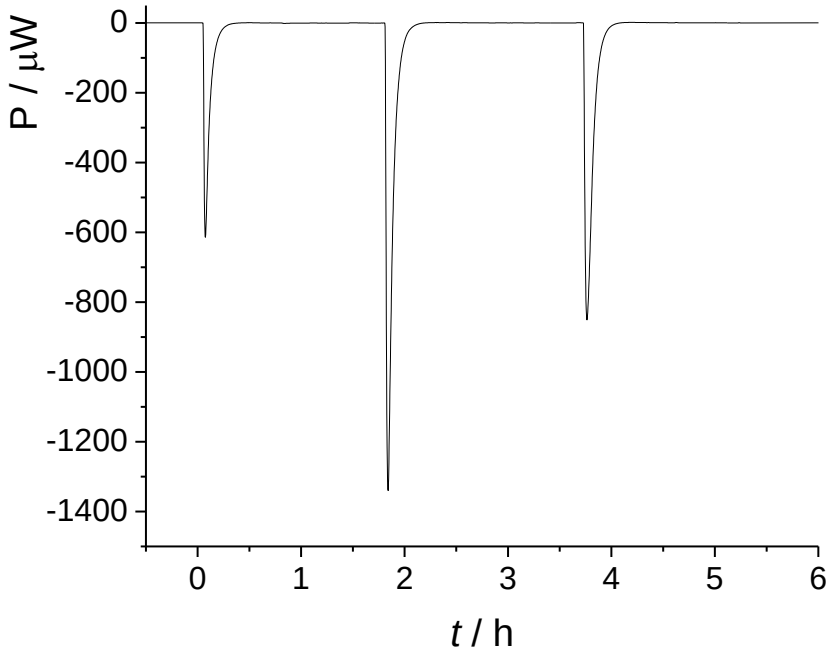

Fig. S12. Calorimetric determination of dissolution enthalpy of **(tftib)(tpss)** (m_1=2.62 mg, m_2=6.12 mg, m_3=4.83 mg) in acetonitrile at 25°C; stirring rate = 60 rpm.

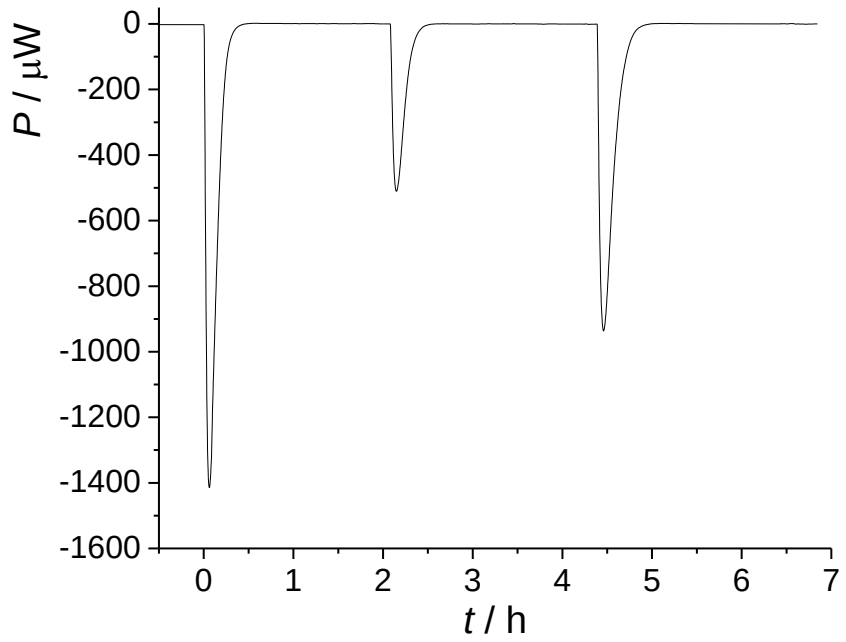

Fig. S13. Calorimetric determination of dissolution enthalpy of **(tpss)** (m_1=7.08 mg, m_2=3.03 mg, m_3=6.35 mg) in acetonitrile at 25°C; stirring rate = 60 rpm.

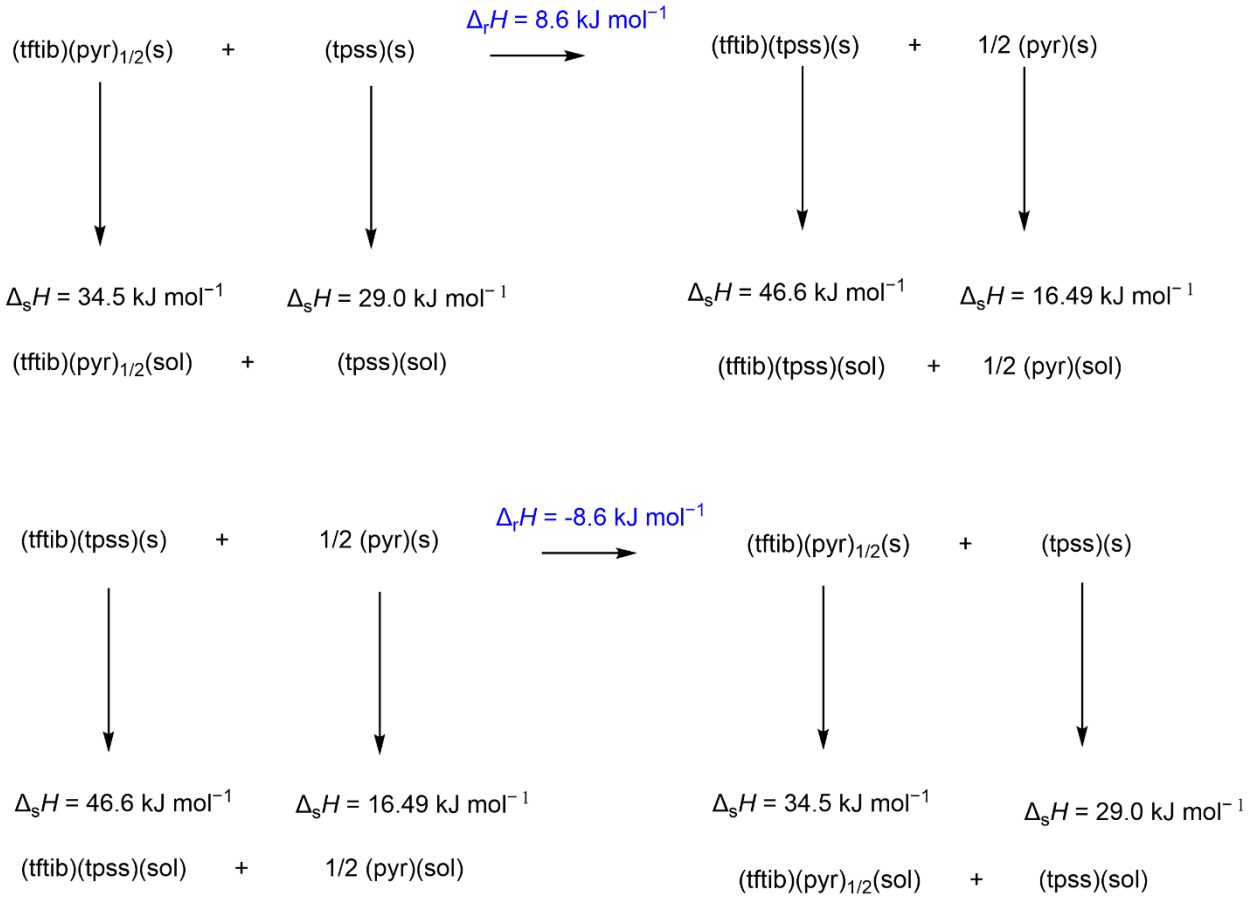

Fig. S14. Thermodynamic cycle for the reactions 1 and 2.

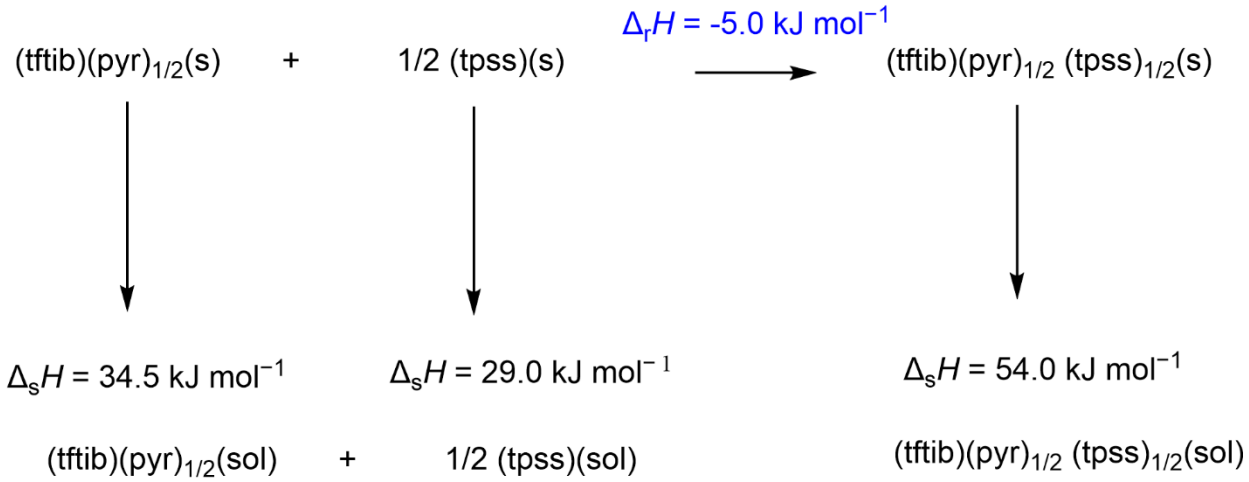

Fig. S15. Thermodynamic cycle for the formation of **3-comp** via reaction 3.

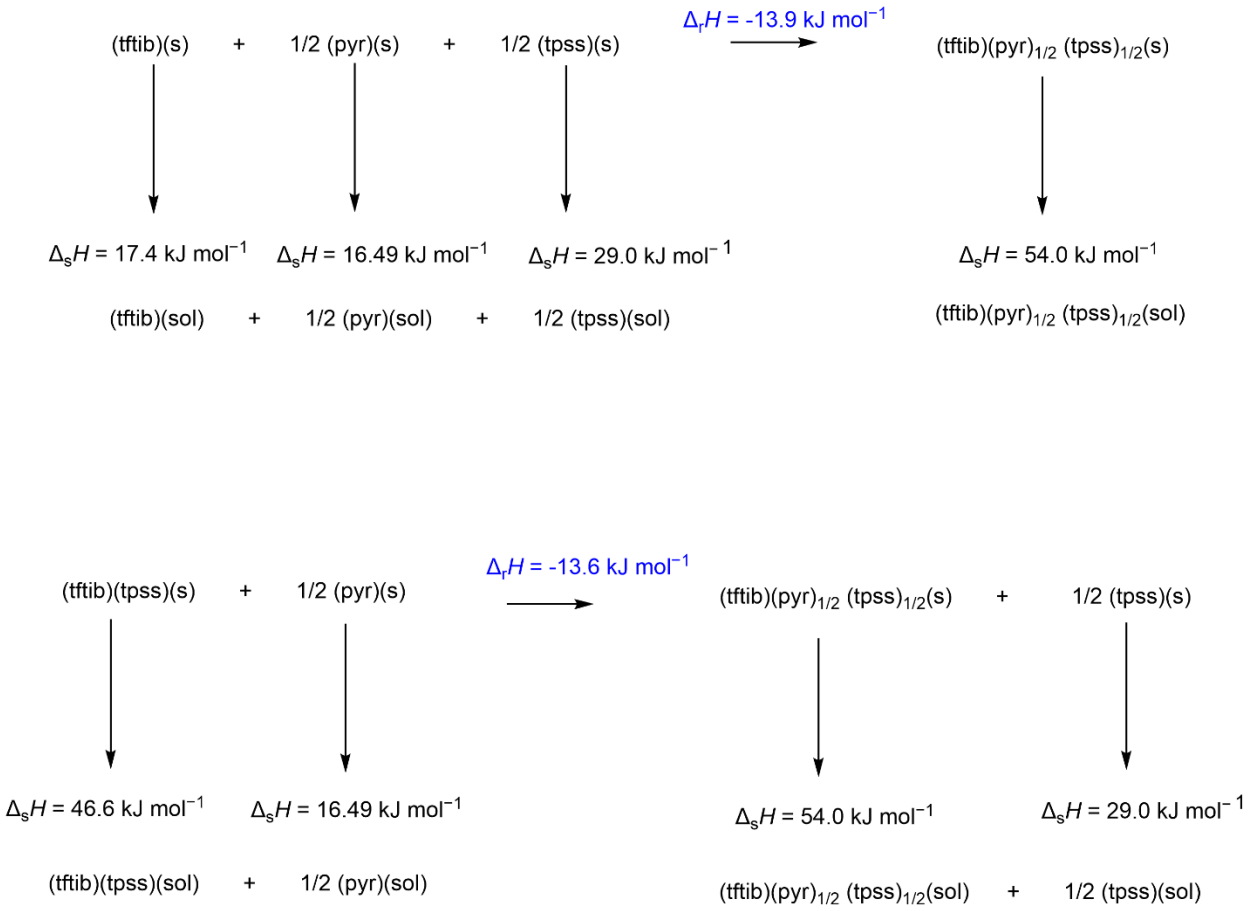

Fig. S16. Thermodynamic cycle for the formation of **3-comp** via reactions 4 and 5.

S4.7 Thermal measurements

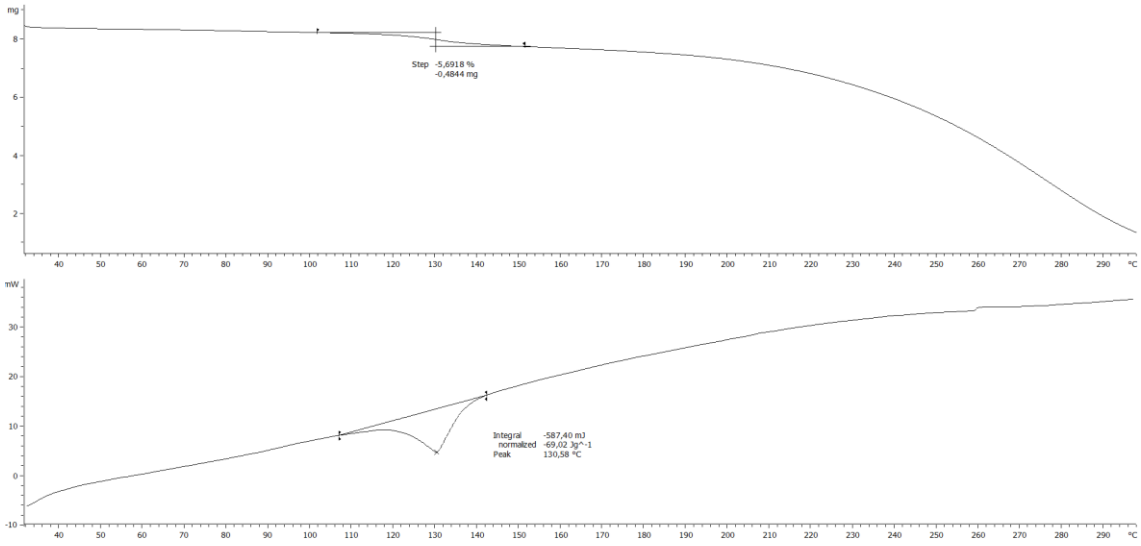

Fig. S17. TGA/DSC curves for the **3-comp**. Observed experimental weight loss (5.69%) at 100−140 ºC, is consistent with the expected weight loss associated with the removal of pyrazine (5.75%). Above weight loss is accompanied by a broad endothermic peak at the DSC curve at 130.58 °C.

S5 References

1. CrysAlis CCD and CrysAlis RED, Oxford Diffraction, Oxford Diffraction Ltd: Yarnton, 2008.
2. R. C. Clark and J. S. Reid, *Acta Crystallogr.*, 1995, **A51**, 887–897.
3. G. M. Sheldrick, *Acta Crystallogr.*, 2008, **A64**, 112–22.
4. C. F. Macrae, I. J. Bruno, J. A. Chisholm, P. R. Edgington, P. McCabe, E. Pidcock, L. Rodriguez-Monge, R. Taylor, J. van de Streek and P. A. Wood, *J. Appl. Crystallogr.*, 2008, **41**, 466–470.
5. L. Kumar, K. Leko, V. Nemec, D. Trzybiński, N. Bregović, D. Cinčić and M. Arhangelskis, *Chem. Sci.*, 2023, **14**, 3140–3146.
6. C. R. Groom, I. J. Bruno, M. P. Lightfoot and S. C. Ward, *Acta Crystallogr.*, 2016, **B72**, 171–179.
7. T. Björkman, *Comput. Phys. Commun.*, 2011, **182**, 1183–1186.
8. J. P. Perdew, M. Ernzerhof and K. Burke, *J. Chem. Phys.*, 1996, **105**, 9982–9985.
9. S. Grimme, J. Antony, S. Ehrlich and H. Krieg, *J. Chem. Phys.*, 2010, **132**, 154104.
10. A. Tkatchenko, R. A. DiStasio, R. Car and M. Scheffler, *Phys. Rev. Lett.*, 2012, **108**, 236402.
11. A. Ambrosetti, A. M. Reilly, R. A. DiStasio and A. Tkatchenko, *J. Chem. Phys.*, 2014, **140**, 18A508.
12. A. M. Reilly and A. Tkatchenko, *Chem. Sci.*, 2015, **6**, 3289–3301.
13. S. J. Clark, M. D. Segall, C. J. Pickard, P. J. Hasnip, M. I. J. Probert, K. Refson and M. C. Payne, *Z. Kristallogr.* 2005, **220**, 567–570.
14. M. J. Turner, S. P. Thomas, M. W. Shi, D. Jayatilaka and M. A. Spackman, *Chem. Commun.*, 2015, **51**, 3735–3738.
15. P. R. Spackman, M. J. Turner, J. J. McKinnon, S. K. Wolff, D. J. Grimwood, D. Jayatilaka and M. A. Spackman, *J. Appl. Crystallogr.*, 2021, **54**, 1006–1011.
16. A. D. Becke, *J. Chem. Phys.*, 1993, **98**, 5648–5652.
17. C. Lee, W. Yang and R. G. Parr, *Phys. Rev. B*, 1988, **37**, 785–789.
18. P. J. Stephens, F. J. Devlin, C. F. Chabalowski and M. J. Frisch, *J. Phys. Chem.*, 1994, **98**, 11623–11627.
19. N. Godbout, D. R. Salahub, J. Andzelm and E. Wimmer, *Can. J. Chem.*, 1992, **70**, 560–571.
20. A. Hasija and D. Chopra, *Cryst. Growth Des.*, 2020, **20**, 6272–6282.